

ENVIRONMENTAL EFFECTS ON REAL-SPACE AND REDSHIFT-SPACE GALAXY CLUSTERING

YING ZU^{1,2}, ZHENG ZHENG^{3,4,5}, GUANGTUN ZHU^{1,6}, AND Y.P. JING¹

Draft version October 24, 2018

ABSTRACT

Galaxy formation inside dark matter halos, as well as the halo formation itself, can be affected by large-scale environments. Evaluating the imprints of environmental effects on galaxy clustering is crucial for precise cosmological constraints with data from galaxy redshift surveys. We investigate such an environmental impact on both real-space and redshift-space galaxy clustering statistics using a semi-analytic model (SAM) derived from the Millennium Simulation. We compare clustering statistics from original SAM galaxy samples and shuffled ones with environmental influence on galaxy properties eliminated. Among the luminosity-threshold samples examined, the one with the lowest threshold luminosity ($\sim 0.2L_*$) is affected by environmental effects the most, which has a $\sim 10\%$ decrease in the real-space two-point correlation function (2PCF) after shuffling. By decomposing the 2PCF into five different components based on the source of pairs, we show that the change in the 2PCF can be explained by the age and richness (galaxy occupation number) dependence of halo clustering. The 2PCFs in redshift space are found to change in a similar manner after shuffling. If the environmental effects are neglected, halo occupation distribution modeling of the real-space and redshift-space clustering may have a less than 6.5% systematic uncertainty in constraining $\sigma_8\Omega_m^{0.6}$ from the most affected SAM sample and have substantially smaller uncertainties from the other, more luminous samples. We argue that the effect could be even smaller in reality. In the Appendix, we present a method to decompose the 2PCF, which can be applied to measure the two-point auto-correlation functions of galaxy sub-samples in a volume-limited galaxy sample and their two-point cross-correlation functions in a single run utilizing only one random catalog.

Subject headings: galaxies: formation — galaxies: halos — large-scale structure of universe — cosmology: theory — dark matter

1. INTRODUCTION

Recently, many authors have identified the environmental impact, which manifests itself as another degree of freedom, on the clustering of halos at fixed mass. Gao et al. (2005) found that low mass halos ($M < M_*$) which formed earlier are more strongly clustered than their younger counterparts; whilst for high mass halos, older halos with $M > 10M_*$ turn out to be less clustered than the younger ones (Wechsler et al. 2006; Jing et al. 2007; Wetzel et al. 2007), where M_* is the nonlinear mass scale for collapse. This environmental dependence of halo clustering, namely “assembly bias” (Gao & White 2007), contradicts with excursion set theory (EST; Bond et al. 1991; Lacey & Cole 1993; Mo & White 1996) which predicts that an individual halo evolves without awareness of the larger environment except for its own mass when it is *observed* (White 1996). In this paper, we investigate the effect of the halo assembly bias on modeling the real-space and redshift-space galaxy clustering statistics and discuss the possible consequence on cosmological parameter constraints from these clustering statistics.

Several possible explanations are proposed to decode halo assembly bias by either studying detailed halo growth within high-resolution N -body simulations or by improving current excursion set theory. Wang et al. (2007) showed that the accretion of low mass halos in dense regions is severely truncated due to tidal disruption and preheating by their massive companions, and Jing et al. (2007) suggested that the competition for accretion resources also triggers a delayed accretion phase which results in the inverse age-dependence of massive halos, while Ariel Keselman & Nusser (2007) argued that highly non-linear effects like tidal stripping may not be the main driver for assembly bias. On the other hand, Zentner (2006) implemented a toy model by substituting the sharp- k filter in EST with a localized configuration one, and Sandvik et al. (2007) integrated EST with ellipsoidal collapse model and barrier-crossing of pancakes and filaments. Both theoretical trials claimed that the assembly bias for massive halos could be naturally recovered, at least partly offset, by deserting Markovian simplification in EST. Recently, Dalal et al. (2008) showed that the assembly bias of rare massive halos is expected from the statistics of peaks in Gaussian random fields, and they argued that the formation of a non-accreting sub-population of low-mass halos is responsible for the assembly bias of low mass halos (also see Hahn et al. 2008).

As the products of gas physics within dark matter halos, galaxies have no reason to be immune from this environmental effect. Croton et al. (2007) and Zhu et al. (2006) showed that environmental effect is transmitted

¹ Shanghai Astronomical Observatory, Joint Institute for Galaxy and Cosmology (JOINGC) of SHAO and USTC, Nandan Road 80, Shanghai, 200030, China; nye@shao.ac.cn ; ypjing@shao.ac.cn.

² Graduate School of the Chinese Academy of Sciences, 19A, Yuquan Road, Beijing, China

³ Institute for Advanced Study, Einstein Drive, Princeton, NJ 08540; zhengz@ias.edu.

⁴ Hubble Fellow.

⁵ John Bahcall Fellow.

⁶ Center for Cosmology and Particle Physics, New York University, New York, NY10003, USA; gz323@nyu.edu.

to the clustering and properties of galaxies in semi-analytic model (SAM) and smoothed particle hydrodynamics (SPH) simulation, both of which extract halo merging histories directly from simulations rather than Markovian process. Observationally, Yang et al. (2006) and Berlind et al. (2006) found a residual dependence of galaxy clustering on group properties other than group mass by using group catalog from the Two-Degree Field Galaxy Redshift Survey (2dFGRS; Colless & et al. 2001) and the Sloan Digital Sky Survey (SDSS; York & et al. 2000), respectively.

In modeling the galaxy clustering, the halo occupation distribution (HOD) or the closely related conditional luminosity function (CLF) is a powerful method to put the observed galaxy clustering in an informative form of describing the relation between galaxies and dark matter halos (Jing et al. 1998; Seljak 2000; Peacock & Smith 2000; Scoccimarro et al. 2001; Cooray & Sheth 2002; Berlind & Weinberg 2002; Yang et al. 2003; Zheng et al. 2005). It successfully explains the departure from a power-law in the observed galaxy two-point correlation functions (Zehavi et al. 2005) and bridges the gap between high-resolution N -body simulations of dark matter particles and large scale surveys of galaxies. HOD modeling also enhances the power of galaxy clustering on constraining cosmological parameters by linking galaxies to dark matter halos and using the clustering data on all scales (van den Bosch et al. 2003; Abazajian et al. 2005; Zheng & Weinberg 2007). However, one key assumption in the current version of the HOD is based on the EST that the formation and the distribution of galaxies within halos are *statistically* determined solely by halo mass. Therefore, it is important to quantify the environmental effect on modeling galaxy clustering within the HOD framework in the era of precision cosmology and provide insights to improve the HOD modeling.

A natural way to study the environmental effect is to extend the current HOD framework by including a second halo variable other than halo mass and compare the modeling results with previous results. Many candidates of halo variables, such as formation time, concentration, substructure richness, and spin, have been scrutinized but all were proved incapable of capturing environmental effect neatly and completely (Gao & White 2007; Wechsler et al. 2006). One of the reasons for this is that halo formation history is subject to incidental merging events and uneven accretion phases, both of which produce a large scatter in the relation between any halo property and the environment (Wechsler et al. 2002; Zhao et al. 2003).

In the present study, we shuffle a semi-analytic galaxy sample to produce three sets of artificial samples, which either partly or completely lost their environmental features, and investigate the changes in real-space and redshift-space galaxy clustering statistics. The shuffling would enable us to see the consequences of neglecting the environmental dependence in the current version of HOD modeling and give us ideas of the effect on constraining cosmological parameters using these statistics (e.g., Tinker et al. 2006). The structure of the paper is as follows. In § 2, we introduce the simulation and the SAM model we use and describe our construction of galaxy samples with different threshold luminosities from the SAM. In § 3, we present three methods of shuffling

the galaxy samples aimed to eliminate the environmental dependence. Then, in § 4, we analyze in detail the effect of environments on the real-space two-point correlation functions (2PCFs) by comparing the results between samples before and after shuffling. In § 5, we study the effect of environments on the redshift-space clustering statistics. We conclude in § 6 with a brief discussion and summary. In the Appendix, we present a method to decompose the 2PCFs into different components based on the properties of galaxy pairs. This method can be generalized to apply to real data to measure the two-point auto-correlation functions of galaxy sub-samples in a volume-limited galaxy sample and their two-point cross-correlation functions in a single run utilizing only one random catalog.

2. SIMULATION DATA AND SEMI-ANALYTIC MODEL

In this study, we make use of outputs from a galaxy formation model based on the Millennium Simulation. The Millennium Simulation (Springel 2005) follows the hierarchical growth of dark matter structures from redshift $z = 127$ to the present. The simulation adopts a concordance cosmological model with $(\Omega_m, \Omega_\Lambda, \Omega_b, \sigma_8, h) = (0.25, 0.75, 0.045, 0.9, 0.73)$, and employs 2160^3 particles of mass $8.6 \times 10^8 h^{-1} M_\odot$ in a periodic box with comoving size $500 h^{-1} \text{Mpc}$ on a side. Friends-Of-Friends (FOF; Davis et al. 1985) halos are identified in the simulation at each of the 64 snapshots with a linking length 0.2 times the mean particle separation. Substructures are then identified by SUBFIND algorithm as locally overdense regions in the background FOF halos (Springel et al. 2001). Detailed merger trees of all gravitationally self-bound dark matter clumps constructed from this simulation provide a key ingredient for semi-analytic models of galaxy formation.

The galaxy catalog we use is from the semi-analytic model (SAM) of De Lucia & Blaizot (2007), which is an updated version of that of Croton et al. (2006) and De Lucia et al. (2006). This model explores a variety of physical processes related to galaxy formation. It can reproduce many observed properties of galaxies in the local universe, including the galaxy luminosity function, the bimodal distribution of colors, the Tully-Fisher relation, the morphology distribution, and the 2PCFs for various type and luminosity selected samples. This particular model is of course not guaranteed to be absolutely right. What is important to our study here is that the environment-dependent ingredients inherent in this model, such as the history of dynamical interactions and mergers of halos, should be well transmitted to and preserved in the resultant galaxy population. We aim to investigate the likely effects of the environmental dependence in this model on galaxy clustering statistics in real space and redshift space and explore the implications for cosmological study with galaxy clustering data.

We construct six luminosity-threshold galaxy samples at $z = 0$ from the SAM catalog according to the rest-frame SDSS r -band absolute magnitude M_r with dust extinction included. Table 1 lists the properties of these samples. Our L207 sample has a number density similar to the observed $L > L_*$ sample (see Table 2 of Zehavi et al. 2005). Since more luminous galaxies tend to reside in more massive halos (e.g., Zehavi et al. 2005), these six samples can probe different halo mass ranges

TABLE 1
PROPERTIES OF THE LUMINOSITY-THRESHOLD SAMPLES

Name	M_r^{\max}	\bar{n} ($10^{-2}h^3\text{Mpc}^{-3}$)	N_{gal}	N_{halo}
L190	-19.0	1.835	2293947	1661007
L200	-20.0	0.771	963452	730330
L207	-20.7	0.293	365845	289226
L210	-21.0	0.167	209206	169864
L217	-21.7	0.032	39402	34129
L220	-22.0	0.013	16084	14148

(from mass below M_* to that above M_*). The halo assembly bias has different amplitudes and signs across these mass ranges (e.g., Gao et al. 2005; Gao & White 2007; Wechsler et al. 2006; Jing et al. 2007), we therefore expect different environmental effects from the six samples.

3. SHUFFLING SCHEMES

Our purpose in this paper is to study the impact of environmental dependence on the HOD modeling of real-space and redshift-space clustering statistics. Besides the six galaxy samples from the SAM, for comparison we also need galaxy samples with the environmental dependence eliminated. Following Croton et al. (2007), we construct such control samples from the original SAM catalog by shuffling galaxy contents in halos of similar masses. We produce three sets of control samples based on three shuffling schemes described below.

We first group all the FOF dark matter halos at $z = 0$ with M_{vir} larger than $5.5 \times 10^{10} h^{-1} M_{\odot}$ in the catalog into different mass bins of width $\Delta \log[M_{\text{vir}}/(h^{-1} M_{\odot})] = 0.1$. Then we record the relative positions and velocities of all the satellites to their affiliated central galaxies, whose positions and velocities are set to those of their host halos in the SAM. Finally, we redistribute the galaxies within individual halo mass bins. The three sets of our control samples (hereafter CTL1, CTL2 and CTL3, respectively) differ in the way how galaxies are re-distributed.

For CTL1, we follow the scheme of Croton et al. (2007) to keep the original configuration of galaxies inside each halo intact and move the galaxy content to its new host as a whole. In this way, the one-halo term contribution to the galaxy clustering statistics is almost unchanged. In order to compensate for the non-zero mass bin effect in the shuffling, we scale the recorded relative position and velocity of each galaxy by $(M_{\text{new}}/M_{\text{old}})^{1/3}$ in order to redistribute the galaxies in the original halo of mass M_{old} to the new host halo of mass M_{new} . This improvement ensures that the position of shuffled galaxy content be regulated by the virial radius of new host halos.

For CTL2, we collect the distance r to the halo center and the velocity v relative to the halo center for all the satellite galaxies that belong to halos in the same mass bin. Then a pair of r and v are randomly drawn from the sets and assigned to a galaxy. This galaxy is put into a randomly selected halo in that mass bin with random orientations for both \mathbf{r} and \mathbf{v} [with the $(M_{\text{new}}/M_{\text{old}})^{1/3}$ scaling applied]. For central galaxies, they are randomly assigned to halos of the same mass bin. This shuffling procedure assumes a mean radial galaxy number density profile for all halos in the same mass bin and completely eliminates any environmental features in the galaxy dis-

tribution inside halos, including the alignment and segregation of satellites, the non-spherical shape of halos, the infall pattern of satellite velocity distribution, and any correlation between central and satellite galaxies (e.g., in luminosity). CTL2 would allow us to infer the largest effect that environment may have on galaxy clustering statistics for the given SAM.

In addition to CTL1 and CTL2, we construct another set of samples (CTL3) by isotropizing satellites inside their own halo without shuffling contents between different halos. In this way, the radial distribution of galaxies in each individual halo is conserved, but the statistical angular distribution loses the anisotropy. CTL3 allows us to isolate the effect of assuming spherical symmetry for the satellite distribution in modeling 2PCFs. Although CTL2 also isotropizes the satellite distribution inside halos, it effectively uses a radial distribution averaged over halos of similar masses. Therefore, comparing CTL3 and CTL2 would show the effect of the scatter in the distributions of satellites in halos of similar masses.

For each of the CTL1, CTL2, and CTL3 shuffling schemes, we create 10 different galaxy catalogs varying the random seed. We extract the 6 control luminosity-threshold samples from each shuffled catalog in accordance with the above L190, L200, L207, L210, L217 and L220 samples of the SAM. To prevent numerical effects from mixing with the physical effects we are to ascertain, we have performed tests by reducing the size of halo mass bins or leaving several most massive bins unshuffled and find that our choice of the bin size does not introduce noticeable numerical effect.

4. ENVIRONMENTAL EFFECT ON REAL-SPACE 2PCFS

We start from comparing the real-space 2PCFs of the original SAM samples and the shuffled samples. The 2PCFs essentially describe the pair count as a function of pair separation. On small (large) scales, galaxy pairs are dominated by one-halo (two-halo) pairs, i.e., intra-halo (inter-halo) pairs.

Our results on the real-space 2PCFs are shown in Figure 1. On small scales ($\lesssim 2h^{-1}\text{Mpc}$), where the one-halo term dominates, 2PCFs from CTL1, CTL2 and CTL3 behave differently. In CTL1, galaxy contents inside halos as a whole are exchanged among halos of similar mass, so we do not expect any appreciable change in the one-halo regime of the 2PCFs. Thus, the small-scale clustering in CTL1 remains almost the same as that of the original one, as seen in Figure 1. The slight differences seen in the plot are a result of the finite mass bin. CTL3 makes satellite distribution inside halos isotropic, which on average enlarge the separations of intra-halo galaxy pairs. So on small scales, 2PCFs of CTL3 are always smaller than those of SAM with a suppression of around 10%. In CTL2, not only the angular distribution of satellite galaxies inside halos are isotropized but the radial galaxy number density profile is averaged within the same mass bin, which completely erases the memories of galaxies about their environments. Figure 1a shows that galaxies in CTL2 exhibit a suppression up to $\sim 10\%$ for L190 samples and the suppression becomes weaker for samples with higher threshold luminosity (e.g., sample L210 in Fig. 1b). The 2PCF for the L217 CTL2 sample (Fig. 1c) is too noisy to tell the trend, but it is likely to still be a suppression (see below).

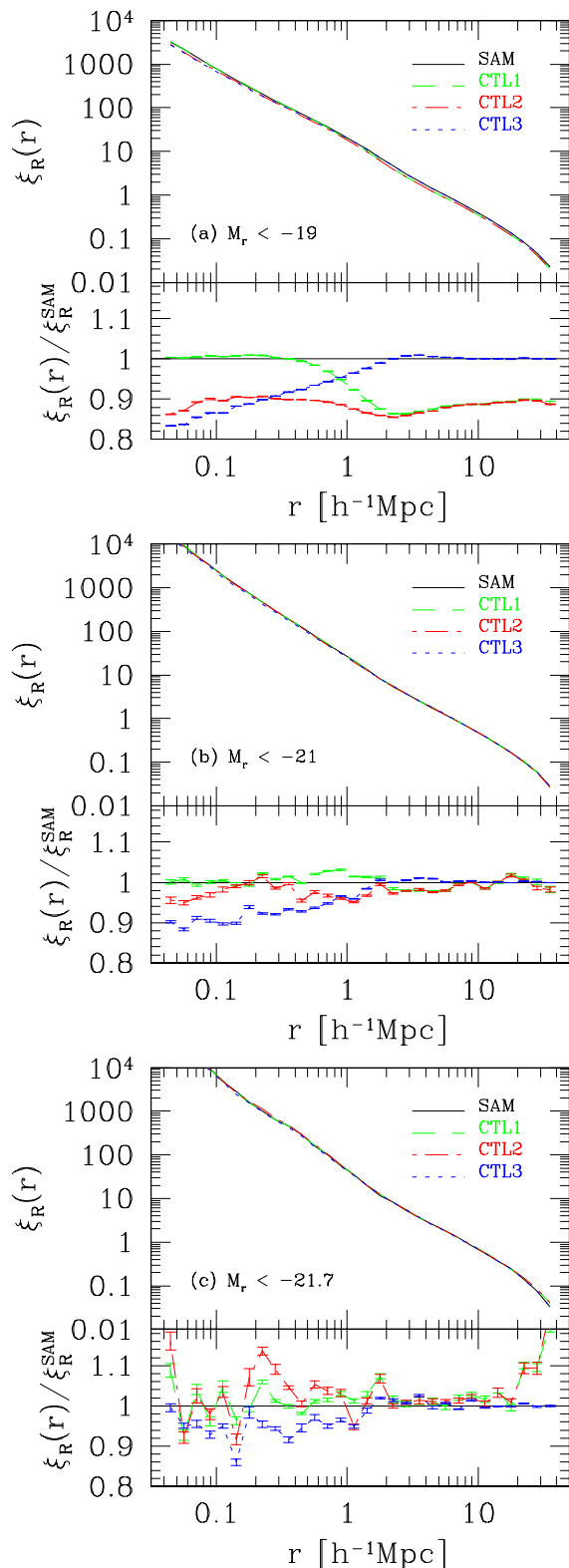


FIG. 1.— The comparison of 2PCFs between SAM and shuffled samples for three different luminosity thresholds. The lower part of each panel gives the ratio of the 2PCFs of the shuffled and the original SAM samples. Solid lines are the 2PCFs for SAM samples, while dashed, dot-dashed, and dotted lines are those for the CTL1, the CTL2 and the CTL3 shuffled samples, respectively. See the text. The (small) error bars reflect the scatter from the 10 realizations for each shuffled sample.

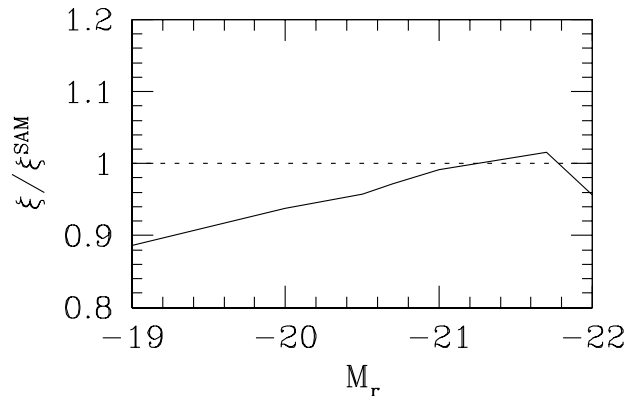


FIG. 2.— The ratio of the 2PCF of shuffled sample to that of the SAM sample as a function of magnitude limit of sample, averaged over scales of $5\text{--}25h^{-1}\text{Mpc}$. In the SAM catalog used in this paper, L_* corresponds to $M_r \sim -20.7$. Since the ratio is nearly constant on those scales, we do not show the small error bars.

On large scales, where the two-halo term dominates, 2PCFs from CTL3 stay the same as those from the original SAM samples, since the CTL3 scheme only shuffles galaxies in each halo. It is not surprising that the large-scale 2PCFs of CTL1 and CTL2 are almost identical, given that they both shuffle halos of similar mass. The difference between the 2PCF in the CTL1/CTL2 sample and the original SAM sample shows a steady trend with the threshold luminosity. For the faint sample ($M_r < -19$), the environmental dependence and the assembly bias lead to a $\sim 10\%$ suppression in the 2PCF after shuffling (Fig. 1a). For the intermediate sample $M_r < -21$, the difference between shuffled and SAM samples is reduced to $\sim 2\%$ (Fig. 1b). For the bright $M_r < -21.7$ sample, the 2PCFs of shuffled ones become $\sim 3\%$ larger than those of the SAM sample (Fig. 1c). To see the trend more clearly, we show in Figure 2 the ratio ξ/ξ^{SAM} of large-scale 2PCFs of the shuffled (CTL1 or CTL2) and the SAM samples as a function of the magnitude limit. The ratio ξ/ξ^{SAM} is calculated by averaging the measurements for each 10 shuffled sample on scales of $5\text{--}25h^{-1}\text{Mpc}$. We note that the trend of the ratio with the threshold luminosity is the same as in Figure 2 of Croton et al. (2007), although we use a different indicator for the large scale difference.

For a better understanding of the change of clustering strength in the shuffled samples with respect to the original samples, we decompose the galaxy 2PCFs into five components according to the source of galaxy pairs and examine them individually. The five components are denoted as 1h-cen-sat, 1h-sat-sat, 2h-cen-cen, 2h-cen-sat, and 2h-sat-sat, where 1h and 2h refer to one-halo and two-halo pairs and cen and sat tell the nature (central or satellite galaxies) of the pair of galaxies. That is, we have central galaxy in a halo paired with satellites in the same halo (1h-cen-sat), satellite galaxy pairs inside halos (1h-sat-sat), central galaxy in one halo paired with central galaxy in a different halo (2h-cen-cen), central galaxy in one halo paired with satellites in a different halo (2h-cen-sat), and satellites in one halo paired with satellites in a different halo (2h-sat-sat). A detailed description on how we separate these components can be found in the Appendix.

Figure 3 shows the five 2PCF components of the orig-

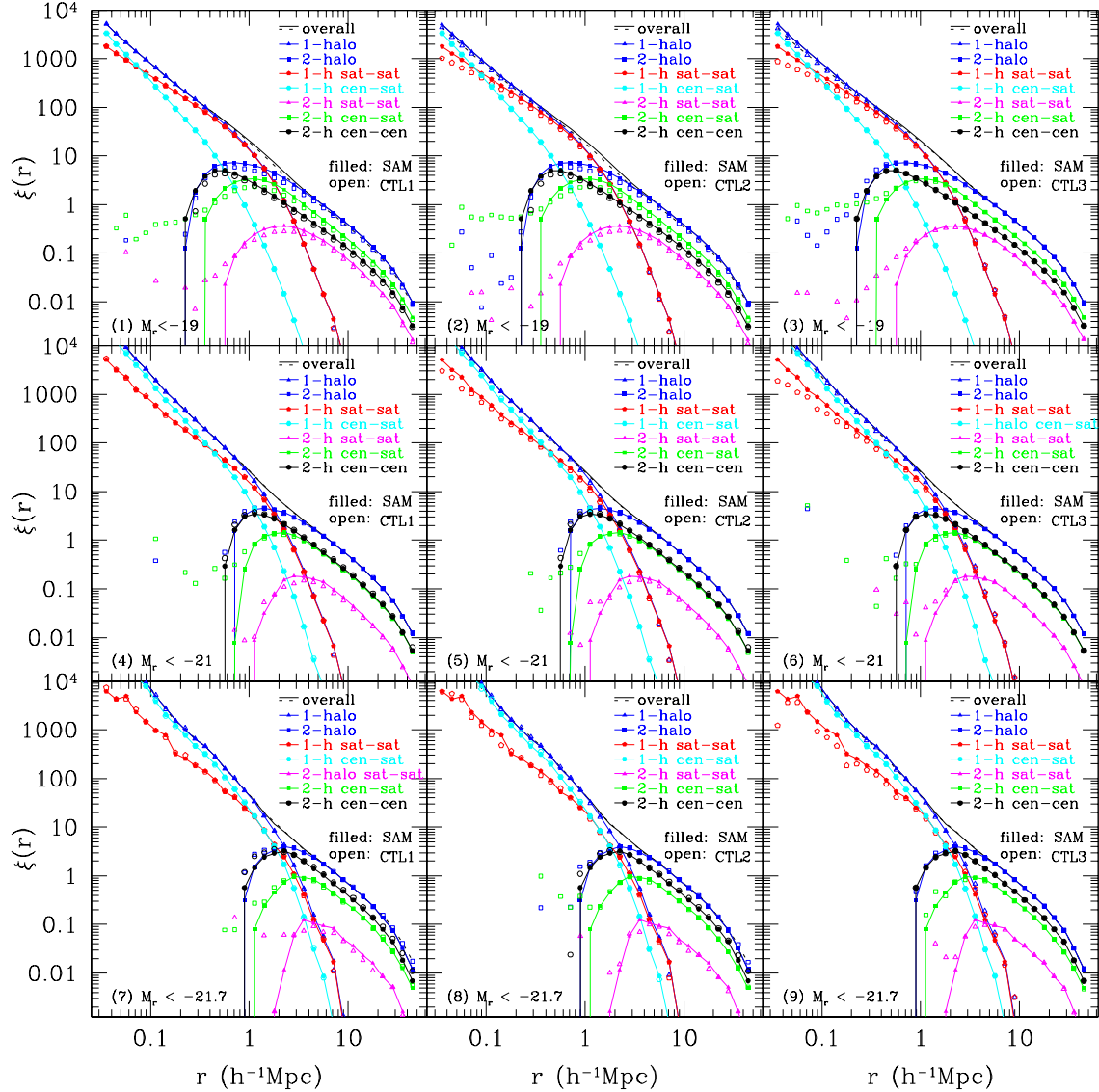


FIG. 3.— Comparison of 2PCFs between SAM and shuffled $M_r < -19$, -21 and -21.7 samples by decomposing the 2PCF into five separate components. Solid and dotted lines are the overall 2PCF for SAM and shuffled samples, respectively. The shuffled sample in the left (middle, right) column is from the CTL1 (CTL2, CTL3) shuffling scheme (see the text). The five components correspond to contributions from one-halo central-satellite galaxy pairs, one-halo satellite-satellite galaxy pairs, two-halo central-central galaxy pairs, two-halo central-satellite galaxy pairs, and two-halo satellite-satellite galaxy pairs, respectively. See the text and the Appendix for more details.

inal and shuffled samples for L190, L210 and L217 (left, middle and right columns for CTL1, CTL2 and CTL3, respectively). Since the spatial distribution of satellites inside halos is conserved in the CTL1 sample [except for the $(M_{\text{new}}/M_{\text{old}})^{1/3}$ scaling], there is almost no change in the one-halo components for this sample with respect to the original sample. In the shuffling schemes of CTL2 and CTL3 samples, satellites inside halos are angularly redistributed from a non-spherical distribution to an isotropic distribution. The redistribution in either CTL2 or CTL3 does not change the separations of one-halo central-satellite galaxy pairs, so the 1h-cen-sat component does not change after shuffling, as seen in Figure 3. However, the isotropization statistically increases the separations of one-halo satellite-satellite pairs and thus dilutes the 1h-sat-sat clustering signal. This leads to a suppression of the 2PCF on small scales with re-

spect to the original sample (e.g., $\sim 10\%$ for L190). CTL2 samples show a smaller suppression in the 1h-sat-sat component than CTL3 samples. There may be two reasons for the difference. First, CTL2 effectively uses a mean radial distribution profile of satellites in halos of a given mass, while CTL3 uses the radial distribution in each individual halo. Because of the scatter in the radial profiles at a given halo mass, the distributions of one-halo satellite-satellite pair separations are not identical from the mean and individual profiles. Second, CTL2 ensures that the numbers of satellites inside halos of a given mass follow the Poisson distribution, while CTL3 follows the distribution in the SAM sample, which can be slightly sub-Poisson in the low occupation regime (e.g., Zheng et al. 2005).

For the shuffled samples CTL1, CTL2 and CTL3, all two-halo components (except 2h-cen-cen) show en-

hancements on scales less than $1h^{-1}\text{Mpc}$ with respect to the original ones. This is mainly caused by the non-spherical distribution of satellite galaxies inside halos in the SAM sample. The shuffling procedure can cause the satellite populations of two neighboring (non-spherical) halos to become spatially close or even overlapped to some extent. Therefore, in the shuffled samples the probability of finding close inter-halo galaxy pairs that involve satellites increases. However, such small-scale enhancements in the two-halo components only occur on scales that the one-halo term of the 2PCF dominates, thus, they are of no interest in our analysis.

On large scales, where the two-halo term regime dominates, the two-halo components for CTL3 do not change since it only shuffles galaxies within halos, while every two-halo component changes its amplitude after shuffling with CTL2 and CTL3. There is no doubt that this should be a manifestation of the environmental dependence of the halo clustering and that of the galaxy content inside halos. Let us first consider the **2h-cen-cen** component. The effect of shuffling central galaxies is equivalent to that of shuffling halos. If the galaxy sample were a halo-mass-threshold sample, shuffling would not change the large scale clustering of central galaxies as the host halo population remains the same after shuffling. However, the sample we consider is defined by a threshold in luminosity and it is not a halo-mass-threshold sample because of the scatter between halo mass and central galaxy luminosity. At a fixed mass, older halos tend to host more luminous central galaxies, and the mean central galaxy luminosity is an increasing function of halo mass (Zhu et al. 2006). We thus expect that, at a given luminosity, a central galaxy can reside in a low mass older halo or in a younger halo of higher mass. That is, for low mass halos, only a fraction of them (some older ones) can host the galaxies in our luminosity-threshold sample. Since the shuffling is among halos of the same mass, some central galaxies of the sample in these low mass older halos are moved to younger halos in the same mass bin after shuffling. For the L190 samples, these low mass halos are in the regime where the clustering of younger halos are weaker, so we see a decrease in the **2h-cen-cen** component of the 2PCF after shuffling [Fig. 3(1) and Fig. 3(2)]. However, halos at the low mass end in L217 samples are in the regime where the clustering of older halos are weaker, leading to an increase in the **2h-cen-cen** component after shuffling [Fig. 3(7) Fig. 3(8)]. For the L210 samples, the low mass halos are in the regime where the age dependence of halo clustering almost disappear, and as a consequence, the **2h-cen-cen** component does not change much after shuffling [Fig. 3(4) and Fig. 3(5)].

Unlike the **2h-cen-cen** component, for which the effect of shuffling is determined by the halos near the low-mass end for the given sample, the **2h-cen-sat** and **2h-sat-sat** components are influenced by all halos above the low-mass end. Zhu et al. (2006) find that, in general, at a fixed halo mass, there are fewer satellite galaxies in older halos. Combining this finding with the age dependence of halo clustering (i.e., older halos being more strongly clustered in the mass range appropriate for our sample), one would infer that shuffling would increase the amplitudes of the **2h-cen-sat** and **2h-sat-sat** components, since the overall effect of shuffling is to homogenize satellite populations among halos of different ages

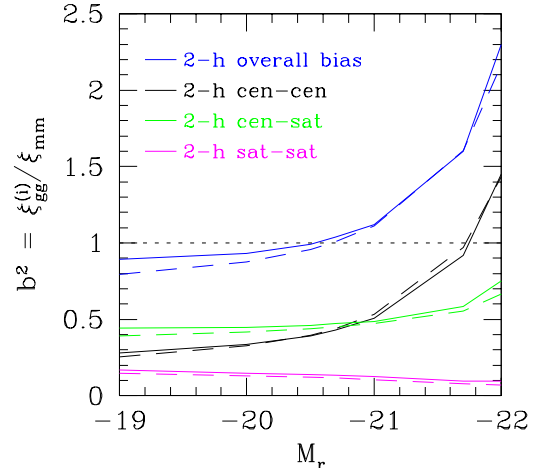


FIG. 4.— Contributions to the large scale bias factor from different pair components as a function of magnitude limit of galaxy sample. The component contribution $\xi_{gg}^{(i)}$ to the large scale 2PCFs, normalized by the matter 2PCF, includes **2h-cen-cen** (black), **2h-cen-sat** (green), and **2h-sat-sat** (magenta). The blue curve is the overall squared bias factor. Solid and dashed lines are for the original SAM and the CTL shuffled samples, respectively. See the text for more details.

(i.e., to increase/decrease the number of satellites in older/younger halos). However, this naive expectation is contradictory to what is seen in Figure 3. Then, what is the reason for the suppression in the **2h-cen-sat** and **2h-sat-sat** components? The answer lies in the richness dependence of halo clustering. Here, the term “richness” refers to subhalo/substructure/satellite abundance in a halo. Gao & White (2007) show that, in the mass range relevant here, halos with more substructures are always more strongly clustered. Since substructures are the natural dwellings of satellite galaxies, we expect that, at a fixed mass, halos that have more satellites are more strongly clustered. The effect of shuffling is to move some satellites in strongly clustered halos to weakly clustered halos and thus lower the amplitude of the **2h-cen-sat** and **2h-sat-sat** components of the 2PCF.

The above explanation of the two-halo term change still leaves with one question. According to the age-dependence of halo clustering (older halos are more strongly clustered) and the anti-correlation between age and subhalo abundance (older halos have fewer subhalos; Gao et al. 2004; Zhu et al. 2006), one would expect that halos with fewer satellites are more strongly clustered, in sharp contrast with what is found in simulation (e.g., Gao & White 2007). The solution to the apparent contradiction lies in the scatter in the anti-correlation between age and richness and the joint dependence of halo clustering on age and richness (Zu et al. in preparation).

Figure 4 summarizes the contributions of two-halo components to the large-scale 2PCFs and the changes caused by CTL1/CTL2 shuffling as a function of threshold luminosity. We plot the contributions from different two-halo components to the large-scale bias factor (squared) for both the original SAM samples (solid) and CTL1 samples (dashed). Each component contribution to the square bias factor is computed by averaging the ratio of the corresponding two-halo 2PCF component (**2h-cen-cen**, **2h-cen-sat**, or **2h-sat-sat**) to the matter 2PCF on scales of $5\text{--}15h^{-1}\text{Mpc}$. For galaxy samples

with low threshold luminosity, the largest contribution to the large-scale clustering comes from the **2h-cen-sat** component. The **2h-cen-cen** component then takes over for samples with threshold luminosity around L_* and becomes more and more dominant towards higher luminosity. This trend can be understood by noticing that the satellite fraction decreases with increasing threshold luminosity (e.g., Zheng et al. 2007). The **2h-sat-sat** component always has the least contribution to the large-scale clustering.

Figure 4 shows that shuffling causes the **2h-cen-cen** component to be suppressed slightly for samples with low luminosity thresholds and to be enhanced a little bit for samples with high luminosity thresholds, a trend can be explained by the age dependence of halo clustering as discussed above. Here “low” and “high” are with respect to L_* . We note that the change in the **2h-cen-cen** component decreases again at the very high luminosity end (i.e., the L220 sample), similar to the trend seen in the concentration dependence of massive halo clustering (see e.g., Jing et al. 2007). The **2h-cen-sat** component is always suppressed after shuffling, which can be understood by the richness dependence of halo clustering as mentioned above. The change of the overall large-scale bias factor is dominated by that of the **2h-cen-sat** at low luminosity and very high luminosity. The change of the **2h-cen-cen** component plays a role in determining that of the overall bias factor for samples with luminosity threshold larger but not much larger than L_* , and it nearly compensates the suppression caused by the change of the **2h-cen-sat** component, leading to little change (<2%) in the overall bias factor (also see Fig. 2).

5. ENVIRONMENTAL EFFECT ON REDSHIFT-SPACE 2PCFS

While the 2PCFs in real space are isotropic, the 2PCFs in redshift space are distorted by galaxy peculiar velocities along the line of sight. On small scales, the random virialized motions of galaxies in groups and clusters stretch the redshift distribution of galaxies along the line of sight, producing the so-called “finger-of-god” (FOG) effect. On large scales, the coherent flows of galaxies due to gravity squash the line-of-sight distribution of galaxies (i.e., Kaiser effect; Kaiser 1987).

In linear theory, the large scale redshift-space distortion measures a combination of Ω_m and the large scale galaxy bias factor b_g , which is $\Omega_m^{0.6}/b_g$. Given the measured amplitude of galaxy 2PCF, a constraint on $\Omega_m^{0.6}/b_g$ is equivalent to that on $\sigma_8\Omega_m^{0.6}$, where σ_8 is the rms matter fluctuation on scale of $8h^{-1}\text{Mpc}$. To infer such a constraint on large scales, the small-scale redshift distortion is usually dealt with simple models, such as the exponential model (Cole et al. 1995). Tinker et al. (2006) demonstrates that by taking advantage of the power of HOD to describe clustering in a fully non-linear manner, one can consistently model the small-scale and the large-scale clustering (also see Tinker 2007). Furthermore, Tinker et al. (2006) shows that the degeneracy in Ω_m and σ_8 from large scale clustering can be broken by making use of the small- and intermediate-scale clustering in redshift space. The HOD framework used in Tinker et al. (2006) assumes no environmental effects on halo clustering and galaxy content inside halos. In § 4, we have shown that in the SAM we use, the real-space

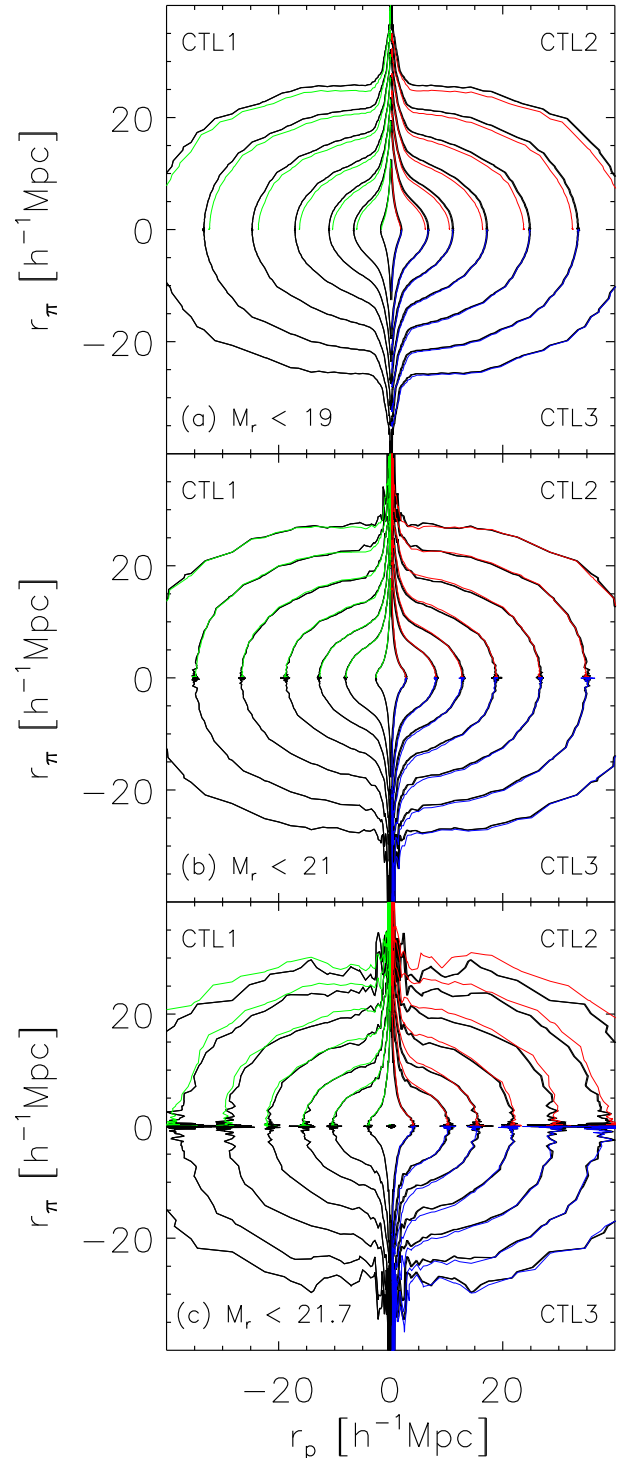


FIG. 5.— Comparison of redshift-space correlation functions between SAM samples and shuffled samples. Panels (a), (b), (c) are for L190, L210, and L217 samples, respectively. In each panel, three quadrants shows the comparison between one shuffled sample and the SAM, with black contours for the original SAM sample, green, red, and blue contours for the CTL1, CTL2, and CTL3 shuffled samples, respectively. Contour levels are set as 2^n , with n from -5 to 2.

2PCFs may suffer a change up to $\sim 10\%$ because of the environmental effect. It is interesting to perform similar analysis in redshift space and discuss the implications in inferring cosmological parameters from redshift distortions.

In Figure 5, we show the redshift-space 2PCFs $\xi(r_p, r_\pi)$ ⁷ measured from the SAM, CTL1, CTL2, and CTL3 catalogs for the three luminosity-threshold samples as in Figure 1, where r_p and r_π are the perpendicular and line-of-sight distances in redshift space. The overall effect of the shuffling on the redshift-space 2PCFs is similar to that seen in the real-space 2PCFs. On small scales, where the FOG effect dominates, the clustering amplitudes of CTL1 samples (green contours) are almost identical to those of the SAM samples (black contours), since shuffling does not change the one-halo term in CTL1. For CTL2 samples (red contours), the FOG effect is slightly suppressed and the small scale clustering is weaker than that of the SAM for L190, but nearly identical to and stronger than that of the SAM for L210 and L217, respectively. For CTL3 samples (blue contours), although they exhibit large difference in real-space 2PCFs, the FOF effect only changes a little, which indicates that the difference caused by galaxy angular distribution is partly masked by the peculiar velocity field on small scales.

On large scales, similar to what is seen in the real-space 2PCFs, at a given large-scales separation (r_p, r_π), the redshift-space 2PCF of CTL1 or CTL2 sample has a lower amplitude than that of the SAM sample for L190; it has an almost identical amplitude to that of the L210 SAM sample; it exceeds that of the L217 SAM sample. The 2PCF amplitudes do not change with CTL3 samples. As a whole, shuffling introduces changes similar to those in the real-space 2PCFs, and these changes can be understood following interpretations in § 4.

To further quantify changes in the redshift-space 2PCFs, we calculate a few statistics derived from the multipoles of the real-space and redshift-space 2PCFs, which were originally proposed by Hamilton (1992). These statistics are also the ones used in the study of Tinker et al. (2006) and Tinker (2007) for HOD modeling the redshift-space distortion.

The multipole moments $\xi_l(r)$ are given by the coefficients of the Legendre polynomial expansion of $\xi(r_p, r_\pi)$.

$$\xi_l(r) = \frac{2l+1}{2} \int_{-1}^{+1} \xi(r_p, r_\pi) P_l(\mu) d\mu \quad (1)$$

where $r = \sqrt{r_p^2 + r_\pi^2}$, $\mu = r_\pi/r$, and $P_l(\mu)$ is the l -th order Legendre polynomial. Based on the multipoles of $\xi(r_p, r_\pi)$, we calculate two statistics. The first one is the ratio of the monopole $\xi_0(r)$ to the real-space 2PCF $\xi_R(r)$,

$$\xi_{0/R}(r) \equiv \frac{\xi_0(r)}{\xi_R(r)}. \quad (2)$$

In linear theory, it is a function of $\beta \equiv \Omega_m^{0.6}/b_g$,

$$\xi_{0/R}(r) = 1 + \frac{2}{3}\beta + \frac{1}{5}\beta^2. \quad (3)$$

⁷ We use the same symbol ξ for both the real-space and redshift-space 2PCFs. Whenever it introduces a confusion, we will add a subscript R for real-space quantities.

The second quantity $Q_\xi(r)$ is related to the quadrupole $\xi_2(r)$,

$$Q_\xi(r) \equiv \frac{\xi_2(r)}{\xi_0(r) - \bar{\xi}_0(r)}, \quad (4)$$

where $\bar{\xi}_0(r)$ is the volume-averaged monopole,

$$\bar{\xi}_0(r) = \frac{3}{r^3} \int_0^r \xi_0(s) s^2 ds. \quad (5)$$

In linear theory, $Q_\xi(r)$ is also a function of β ,

$$Q_\xi(r) = \frac{\frac{4}{3}\beta + \frac{4}{7}\beta^2}{1 + \frac{2}{3}\beta + \frac{1}{5}\beta^2}. \quad (6)$$

Tinker et al. (2006) also introduce a quantity $r_{\xi/2}$, which is the value of r_π at which the redshift-space 2PCF at the given r_p decreases by a factor of 2 with respect to the value of 2PCF at $r_\pi = 0$. We also compute this quantity.

Figure 6 plots $\xi_{0/R}$ and Q_ξ as a function of r and $r_{\xi/2}$ as a function of r_p for the L190 sample using both linear and logarithmic axes to highlight large and small scales separately. According to the above results, this sample, among the six luminosity-threshold samples, is expected to show the largest environmental effect (we also check the luminosity-threshold sample with magnitude limit $M_r = -18.0$ and find that the large scale suppression is still at the 10% level as it is in L190).

Compared to the SAM sample, the monopole term $\xi_{0/R}$ in either CTL1 or CTL2 is only $\sim 2\%$ higher on large scales, where it stays the same in CTL3. On small scales ($0.1-1h^{-1}\text{Mpc}$), the difference is at a level of 5% in CTL1&2. Only on extremely small scales ($\lesssim 0.1h^{-1}\text{Mpc}$) does $\xi_{0/R}$ of the CTL2 sample show a 10% drop, which is not important since the error bars are large and these scales are likely to be excluded in HOD modeling. In the CTL3 sample, since the suppression of the spherically-averaged redshift-space 2PCFs and that of the real-space 2PCFs cancel with each other on small scales, $\xi_{0/R}$ stays at the same level as in the SAM sample.

For the quadrupole term Q_ξ , the difference between the results of the original and shuffled samples is well within 5.5% in CTL1/CTL2 for most scales. Note that the difference extends all the way to the largest scales in CTL3 at a 0.5% level, which means that the non-linearity still affects clustering behaviors on linear scales in redshift-space. Also note that the large fractional differences around $10h^{-1}\text{Mpc}$ are simply because Q_ξ is crossing zero. The fractional changes in $\xi_{0/R}$ and Q_ξ caused by shuffling are much less than those in the real-space 2PCFs, which are at a level of 10%. For the quantity $r_{\xi/2}$, the global enhancement in CTL3 is caused only by the angular isotropizing of galaxies, which disrupts the original compact configuration of SAM halos. This makes the redshift-space 2PCFs harder to decrease to the half value of $\xi|_{r_\pi=0}$ at a given r_p , especially at $r_p < 0.2h^{-1}\text{Mpc}$, where the enhancement becomes much eminent. In CTL2, $r_{\xi/2}$ shows a similar behavior as in CTL3 at small r_p for the same reason, then it becomes smaller than that in CTL3 at $r_p > 0.2h^{-1}\text{Mpc}$, while $r_{\xi/2}$ from the CTL1 shuffled sample is consistent with that from the original sample within the error bars.

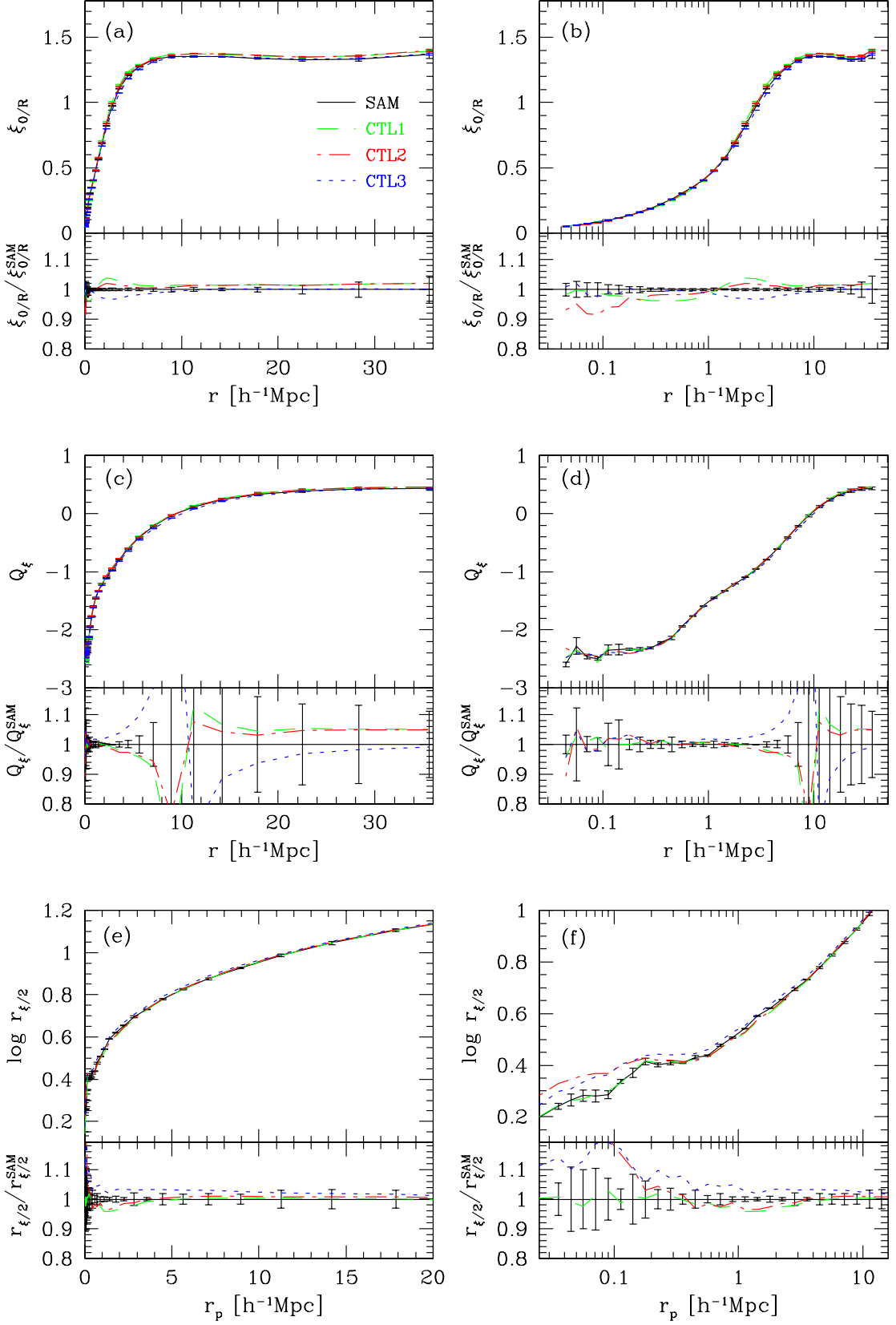


FIG. 6.— Comparison of redshift-space clustering statistics between the SAM and shuffled samples for the L190 galaxy sample. Top panels are for $\xi_{0/R}$, the ratio of the monopole of the redshift-space 2PCF to the real-space 2PCF; middle panels are for Q_ξ , which is related to the quadrupole of the redshift-space 2PCF; bottom panels are for $r_{\xi/2}$, which is the value of r_π at which the redshift-space 2PCF at a given r_p decreases by a factor of 2 relative to its value at $r_\pi = 0$. In each panel, black solid curves stand for the SAM sample, while the green dashed, the red dot-dashed and the blue dotted curves indicate the CTL1, CTL2, and CTL3 shuffled samples, respectively. The horizontal axes are shown in linear (logarithmic) scales in the left (right) panels to highlight the large (small) scale behavior. Error bars are plotted only for the SAM sample to avoid crowding and those for the shuffled ones are comparable. The abnormal error bars around $10 h^{-1}\text{Mpc}$ in the middle panels of panels (c) and (d) are because of Q_ξ there approaching zero.

How would the above changes in the redshift distortion statistics induced by the environmental effect affect the inference of cosmological parameters from HOD modeling? For a complete answer of this question, one needs to perform the analysis presented in Tinker (2007) with the 2PCF measurements in the original and shuffled samples and compare the results in the inferred cosmological parameters. However, even without the full analysis, we can still figure out the likely magnitude by using the linear theory results [equations (3) and (6)]. For the L190 sample presented in Figure 6, a 2% increase in the large-scale $\xi_{0/R}$ only leads to $\sim 6.5\%$ increase in the inferred β . For Q_ξ , shuffling gives rise to a 5.5% increase on large scales, which also translates to a $\sim 6.5\%$ increase in β . For $r_{\xi/2}$, it is not straightforward to see the consequence. Based on Figure 16 of Tinker et al. (2006), it is likely that the difference in $r_{\xi/2}$ on large scales between the SAM and shuffle samples can at most lead to a $\sim 5\%$ uncertainty in constraining σ_8 . We note that the effects of the shuffling on both the real-space and redshift-space clustering statistics are likely from the same cause in that the $\sim 12\%$ decrease in the real-space 2PCF $\xi_R(r)$ leads to 6% decrease in galaxy bias b_g , which in turn corresponds to a $\sim 6.5\%$ increase in β , about the number we infer from redshift-space clustering statistics. Since the shuffling induced changes in the real-space 2PCFs for other brighter samples are smaller, the environmental effect on β is expected to be smaller for them. Therefore, in the SAM galaxy catalog we use, neglecting any environmental dependence of halo clustering and galaxy formation is likely to cause a less than 7% systematic uncertainty in constraining $\sigma_8\Omega_m^{0.6}$.

6. SUMMARY AND DISCUSSION

In this work, we investigate the effect of environmental dependence of halo clustering and galaxy formation on real-space and redshift-space clustering of galaxies. Our study makes use of the galaxy catalog from the SAM of De Lucia & Blaizot (2007), which is based on the Millennium Simulation (Springel 2005). The inherent dependence of galaxy properties on environment in the SAM catalog is eliminated by shuffling galaxies among halos of similar mass.

The real-space 2PCFs in the original sample and those in the shuffled samples have a difference at the level of 10% with some dependencies on scales for samples with low threshold luminosities. The difference becomes much smaller for samples with threshold luminosities approaching or exceeding L_* . We decompose the 2PCFs into five components by accounting for the nature of galaxy pairs (e.g., one-halo or two-halo, central galaxies or satellites) and study the effect of environment on each of them. In general, on large scales, the changes in the **2h-cen-cen** component of the 2PCF caused by shuffling can be well understood by noticing the dependence of halo bias and central galaxy luminosity on halo formation time, while those in the **2h-cen-sat** and **2h-sat-sat** components are determined by the richness (substructure) dependence of halo bias. The **2h-cen-sat** component appears to dominate the change in the overall 2PCF for samples with low or very high threshold luminosity, while the change in the **2h-cen-cen** component nearly compensates that in the **2h-cen-sat** component

for threshold luminosity L_* , where the amplitude of the environment effect is small. These results imply that we could use high-resolution N -body simulations to accurately model the 2PCFs by associating satellites to substructures identified in halos and neglecting the environmental dependence of central galaxies at fixed halo mass. On small scales, the assumption of spherical symmetry in galaxy distribution may lead to an uncertainty as large as 10% in 2PCFs, but this effect could be absorbed into a free parameter describing the halo concentration.

The effects of environmental dependence on redshift-space 2PCFs are similar to what are seen in the real-space 2PCFs. On large scales, the effects can be attributed solely to the change in the large scale bias factor. For inferring cosmological parameters (σ_8 and Ω_m) through HOD modeling of the redshift-space distortion (Tinker et al. 2006; Tinker 2007), the systematic effect caused by neglecting the environmental dependence of halo clustering and galaxy formation is likely to be at the level of $< 6.5\%$ for the worst case (the $M_r < -19.0$ or $L > 0.2L_*$ sample) and can be much smaller for brighter samples, especially for samples with threshold luminosities near L_* . The underlying assumption of this statement is that the environmental effect on galaxy formation in reality is as large as that seen in the SAM we use in this paper.

Our results are based on one particular galaxy formation model, i.e., SAM of De Lucia & Blaizot (2007). Although this model can reproduce many observed properties of galaxies, it is not guaranteed to be absolutely correct. In this model, the environmental effect on the formation and evolution of galaxies is mostly linked to the formation/merger history of dark matter halos. Compared to observations, it overproduces faint red galaxies (Croton et al. 2006). Although the model predicts the correct trend of the color dependent galaxy clustering, it predicts too large a difference between the amplitudes of the 2PCFs of blue and red galaxies (Springel 2005). By comparing to the galaxies in SDSS groups, Weinmann et al. (2006) find that SAM produces too many faint satellites in massive halos and incorrect blue fractions of central and satellite galaxies.

The discrepancies between observations and the SAM model suggest that the effect of environment on galaxy formation and evolution may be exaggerated in this particular model. Such discrepancies provide opportunities for enhancing our understanding of galaxy formation and evolution. There are also tests with void statistics (Tinker et al. 2007), environmental dependence of group galaxies (Blanton & Berlind 2007), and marked galaxy correlation function (Skibba et al. 2006), which show that the observed properties of galaxies are mainly driven by host halo mass rather than the environment in which halos form. Therefore, in reality, it is quite possible that the environmental effect on modeling galaxy clustering statistics is much smaller than what we obtain in this paper, and that the systematic effect on cosmological parameter constraints from HOD modeling is not larger than a few percent or even better.

We thank Jeremy Tinker for helpful discussions and David Weinberg for useful comments. Y. Z. and Y. P. J. are supported by NSFC (10533030), by the Knowledge

Innovation Program of CAS (No. KJ CX2-YW-T05), by 973 Program (No.2007CB815402), and by Shanghai Key Projects in Basic research (05XD14019). At an earlier stage of this work, Z. Z. was supported by NASA through Hubble Fellowship grant HF-01181.01-A awarded by the Space Telescope Science Institute, which is operated by the Association of Universities for Research in Astronomy, Inc., for NASA, under contract NAS 5-26555. Z.

Z. gratefully acknowledges support from the Institute for Advanced Study through a John Bahcall Fellowship. The Millennium Simulation databases used in this paper and the web application providing online access to them were constructed as part of the activities of the German Astrophysical Virtual Observatory.

APPENDIX

DECOMPOSITION OF THE TWO-POINT CORRELATION FUNCTION

In the HOD framework, the 2PCF $\xi(r)$ is usually decomposed into two components (e.g., Zheng 2004),

$$\xi(r) = [1 + \xi_{1h}(r)] + \xi_{2h}(r), \quad (\text{A1})$$

where the one-halo term $\xi_{1h}(r)$ and the two-halo term $\xi_{2h}(r)$ represent contributions from intra-halo and inter-halo pairs, respectively. To separate such components from measurements in a mock catalog, one only needs to weigh the total correlation function appropriately. That is, $1 + \xi(r)$ weighted by the fraction of intra-halo (inter-halo) pairs at a separation r gives $1 + \xi_{1h}(r)$ [$1 + \xi_{2h}(r)$]. However, the way to decompose $\xi(r)$ into more components on the basis of pair counts, like what we do in this paper (central/satellite, one-halo, two-halo pairs), is not immediately clear. In this Appendix, we develop a method for such a decomposition. The method can be generalized to apply to real data: for example, one is able to measure the two-point auto-correlation functions of red and blue galaxies and their two-point cross-correlation functions in a single run with only one random catalog.

We first provide a general consideration on the component separation and then describe the decomposition used in this paper in more details.

General Consideration

Let us start from the definition of the two-point correlation function,

$$\xi(\mathbf{r}) = \langle \delta(\mathbf{x})\delta(\mathbf{x} + \mathbf{r}) \rangle, \quad (\text{A2})$$

where $\langle \dots \rangle$ represents an ensemble average. The overdensity field δ is defined as

$$\delta(\mathbf{x}) = \frac{n(\mathbf{x}) - \bar{n}}{\bar{n}}, \quad (\text{A3})$$

where $n(\mathbf{x})$ is the galaxy density at \mathbf{x} and \bar{n} is the mean. Let us assume that the galaxy sample is composed of several sub-samples, $n(\mathbf{x}) = \sum_i n_i(\mathbf{x})$. Now we decompose the overdensity into different components based on sub-samples

$$\delta = \sum_i \tilde{\delta}_i, \quad (\text{A4})$$

where $\tilde{\delta}_i$ is the overdensity contributed by the i -th component (sub-sample),

$$\tilde{\delta}_i = \frac{n_i - \bar{n}_i}{\bar{n}} = \frac{n_i - \bar{n}_i}{\bar{n}_i} \times \frac{\bar{n}_i}{\bar{n}} = \delta_i \frac{\bar{n}_i}{\bar{n}}. \quad (\text{A5})$$

Note that in the above equation, δ_i is the i -th component's own overdensity field (i.e., fractional fluctuation with respect to \bar{n}_i instead of \bar{n}).

Substituting equations (A4) and (A5) into (A2), we obtain

$$\xi(\mathbf{r}) = \sum_i \langle \delta_i(\mathbf{x})\delta_i(\mathbf{x} + \mathbf{r}) \rangle \frac{\bar{n}_i^2}{\bar{n}^2} + \sum_{i < j} \langle \delta_i(\mathbf{x})\delta_j(\mathbf{x} + \mathbf{r}) \rangle \frac{2\bar{n}_i\bar{n}_j}{\bar{n}^2}. \quad (\text{A6})$$

That is, the total correlation function is a weighted sum of the auto- and cross-correlation functions of all components, where the weight is the pair fraction. In terms of measurement from pair counts in a galaxy catalog and an auxiliary random catalog, it converts to

$$\xi(\mathbf{r}) = \sum_{i \leq j} \frac{dd_{ij}(\mathbf{r}) - rr_{ij}(\mathbf{r})}{rr_{ij}(\mathbf{r})} f_{ij}, \quad (\text{A7})$$

where dd_{ij} and rr_{ij} are the ij data-data and random-random pairs. The quantity f_{ij} is the overall ij pair fraction (the ratio of the total number of ij pairs in the volume to that of all pairs in the volume). Note that, for random pairs, the ratio of the number of random ij pairs to that of all random pairs is independent of separation, i.e., $f_{ij} = rr_{ij}(\mathbf{r})/RR(\mathbf{r})$, where RR is the number of random pairs for all galaxies. Therefore, we have the contribution from the ij component as

$$\xi_{ij}(\mathbf{r}) = \frac{dd_{ij}(\mathbf{r}) - rr_{ij}(\mathbf{r})}{RR(\mathbf{r})}, \quad (\text{A8})$$

where rr_{ij}/RR is a known quantity given the number density of each component and one only needs to measure $dd_{ij}(\mathbf{r})$ and $RR(\mathbf{r})$.

An interesting application of the above results to real data is to measure 2PCFs (either projected ones or redshift-space ones) of sub-samples of galaxies of a volume-limited sample (e.g., a sample of galaxies divided into blue, green, and red galaxy sub-samples). To measure all the two-point auto-correlation functions of galaxies in the sub-samples and their two-point cross-correlation functions, we do not need to construct random catalogs for each sub-sample. We only need one random catalog for the whole sample and measure all the correlation functions in a single run based on equation (A8). The two-point auto-correlation function for all the galaxies in the whole sample, as the weighted sum of the two-point auto- and cross-correlation functions of sub-samples (eq.[A6]), is obtained for free. To generalize equation (A8) in the spirit of the widely used Landy-Szalay estimator (Landy & Szalay 1993), one can replace $-rr_{ij}(\mathbf{r})$ with $-2dr_{ij}(\mathbf{r}) + rr_{ij}(\mathbf{r})$. To count dr_{ij} data-random pairs, one may randomly tag the points in the random catalog with component indices according to the fraction of the sub-sample galaxy spatial density in the overall sample.

Details on the Decomposition of the 2PCF into Central/Satellite and One-halo/Two-halo Terms

Following similar reasoning as in § A.1, now let us tag galaxies with two subscripts and decompose the overdensity field as

$$\delta = \sum_{i,\alpha} \tilde{\delta}_{i\alpha}, \quad (\text{A9})$$

where i denotes the ID of the host halo and α is either c (central) or s (satellite). That is, the overdensity is decomposed into contributions from central and satellite galaxies from each halo. The random catalog can be obtained by randomly redistributing all the galaxies in the volume with their tags untouched.

In a similar way as before, we can write $\tilde{\delta}_{i\alpha}$ as

$$\tilde{\delta}_{i\alpha} = \frac{n_{i\alpha} - \bar{n}_{i\alpha}}{\bar{n}_{i\alpha}} \times \frac{\bar{n}_{i\alpha}}{\bar{n}} = \delta_{i\alpha} \frac{\bar{n}_{i\alpha}}{\bar{n}}. \quad (\text{A10})$$

It is straightforward to show that $\xi(\mathbf{r})$ can be formally decomposed as

$$\begin{aligned} \xi(\mathbf{r}) = & \sum_i \langle \delta_{ic}(\mathbf{x}) \delta_{ic}(\mathbf{x} + \mathbf{r}) \rangle \frac{\bar{n}_{ic}^2}{\bar{n}^2} \\ & + \sum_i \langle \delta_{ic}(\mathbf{x}) \delta_{is}(\mathbf{x} + \mathbf{r}) \rangle \frac{2\bar{n}_{ic}\bar{n}_{is}}{\bar{n}^2} \\ & + \sum_i \langle \delta_{is}(\mathbf{x}) \delta_{is}(\mathbf{x} + \mathbf{r}) \rangle \frac{\bar{n}_{is}^2}{\bar{n}^2} \\ & + \sum_{i<j} \langle \delta_{ic}(\mathbf{x}) \delta_{jc}(\mathbf{x} + \mathbf{r}) \rangle \frac{2\bar{n}_{ic}\bar{n}_{jc}}{\bar{n}^2} \\ & + \sum_{i\neq j} \langle \delta_{ic}(\mathbf{x}) \delta_{js}(\mathbf{x} + \mathbf{r}) \rangle \frac{\bar{n}_{ic}\bar{n}_{js}}{\bar{n}^2} \\ & + \sum_{i<j} \langle \delta_{is}(\mathbf{x}) \delta_{js}(\mathbf{x} + \mathbf{r}) \rangle \frac{2\bar{n}_{is}\bar{n}_{js}}{\bar{n}^2}. \end{aligned} \quad (\text{A11})$$

It is easy to identify the six terms in the right hand side as contributions from the one-halo cen-cen (which is a Dirac δ_D function that we are not interested in), the one-halo cen-sat, the one-halo sat-sat, the two-halo cen-cen, the two-halo cen-sat, and the two-halo sat-sat pairs, respectively (‘cen’ for central galaxy and ‘sat’ for satellite galaxy).

In terms of measurement, each component can be reduced to the $(dd - rr)/RR$ form. As an example, consider the case for the two-halo cen-sat term. Note that $\bar{n}_{ic} = 1/V$, $\bar{n}_{is} = N_{is}/V$, and $\bar{n} = N/V$, where N_{is} is the number of satellites in the halo of ID i and N is the total number of all galaxies in the volume V . Therefore, the two-halo cen-sat contribution is

$$\xi_{2h,cs}(\mathbf{r}) = \sum_{i\neq j} \langle \delta_{ic}(\mathbf{x}) \delta_{js}(\mathbf{x} + \mathbf{r}) \rangle \frac{\bar{n}_{ic}\bar{n}_{js}}{\bar{n}^2} = \sum_{i\neq j} \frac{dd_{ic,js}(\mathbf{r}) - rr_{ic,js}(\mathbf{r})}{rr_{ic,js}(\mathbf{r})} \frac{N_{js}}{N^2}, \quad (\text{A12})$$

where $dd_{ic,js}$ and $rr_{ic,js}$ are numbers of data-data and random-random pairs between galaxies tagged as ic and js . One thing to notice is that $2rr_{ic,js}(\mathbf{r})/N_{js}$ does not depend on i and j — it equals $rr_{cs'}(\mathbf{r})/N_{\text{pair},cs'}$, where $rr_{cs'}(\mathbf{r}) = \sum_{i\neq j} rr_{ic,js}(\mathbf{r})$ is the count of all the random “two-halo” cen-sat pairs with separation around \mathbf{r} and $N_{\text{pair},cs'}$ is the total number of “two-halo” cen-sat pairs in the volume (cs' denotes a “two-halo” pair). Also noting that $N^2/2 = N_{\text{pair},total}$ ($N \gg 1$), we then have

$$\xi_{2h,cs}(\mathbf{r}) = \frac{dd_{cs'}(\mathbf{r}) - rr_{cs'}(\mathbf{r})}{rr_{cs'}(\mathbf{r})/N_{\text{pair},cs'}} \frac{1}{N_{\text{pair},total}}, \quad (\text{A13})$$

where $dd_{cs'}$ and $rr_{cs'}$ are all the data-data and random-random “two-halo” cen-sat pairs with separation around \mathbf{r} . We have the following relation between $rr_{cs'}$ and the total number of all random pairs around separation \mathbf{r} , $RR(\mathbf{r})$,

$$\frac{rr_{cs'}(\mathbf{r})}{N_{\text{pair},cs'}} = \frac{RR(\mathbf{r})}{N_{\text{pair},total}}. \quad (\text{A14})$$

Therefore, we end up with

$$\xi_{2h,cs}(\mathbf{r}) = \frac{dd_{cs'}(\mathbf{r}) - rr_{cs'}(\mathbf{r})}{RR(\mathbf{r})}. \quad (\text{A15})$$

REFERENCES

- Abazajian, K., Zheng, Z., Zehavi, I., Weinberg, D. H., Frieman, J. A., Berlind, A. A., Blanton, M. R., Bahcall, N. A., Brinkmann, J., Schneider, D. P., & Tegmark, M. 2005, *ApJ*, 625, 613
- Berlind, A. A., Kazin, E., Blanton, M. R., Pueblas, S., Scoccimarro, R., & Hogg, D. W. 2006, *ArXiv Astrophysics e-prints*
- Berlind, A. A., & Weinberg, D. H. 2002, *ApJ*, 575, 587
- Blanton, M. R., & Berlind, A. A. 2007, *ApJ*, 664, 791
- Bond, J. R., Cole, S., Efstathiou, G., & Kaiser, N. 1991, *ApJ*, 379, 440
- Cole, S., Fisher, K. B., & Weinberg, D. H. 1995, *MNRAS*, 275, 515
- Colless, M., & et al. 2001, *MNRAS*, 328, 1039
- Cooray, A., & Sheth, R. 2002, *Phys. Rep.*, 372, 1
- Croton, D. J., Gao, L., & White, S. D. M. 2007, *MNRAS*, 374, 1303
- Croton, D. J., Springel, V., White, S. D. M., De Lucia, G., Frenk, C. S., Gao, L., Jenkins, A., Kauffmann, G., Navarro, J. F., & Yoshida, N. 2006, *MNRAS*, 365, 11
- Dalal, N., White, M., Bond, J. R., & Shirokov, A., 2008, *ArXiv Astrophysics e-prints*
- Davis, M., Efstathiou, G., Frenk, C. S., & White, S. D. M. 1985, *ApJ*, 292, 371
- De Lucia, G., & Blaizot, J. 2007, *MNRAS*, 375, 2
- De Lucia, G., Springel, V., White, S. D. M., Croton, D., & Kauffmann, G. 2006, *MNRAS*, 366, 499
- Gao, L., Springel, V., & White, S. D. M. 2005, *MNRAS*, 363, L66
- Gao, L., & White, S. D. M. 2007, *MNRAS*, L19+
- Gao, L., White, S. D. M., Jenkins, A., Stoehr, F., & Springel, V. 2004, *MNRAS*, 355, 819
- Hahn, O., Porciani, C., Dekel, A., & Carollo, C. M. 2008, *ArXiv e-prints*, 803, arXiv:0803.4211
- Hamilton, A. J. S. 1992, *ApJ*, 385, L5
- Jing, Y. P., Mo, H. J., & Boerner, G. 1998, *ApJ*, 494, 1
- Jing, Y. P., Suto, Y., & Mo, H. J. 2007, *ApJ*, 657, 664
- Kaiser, N. 1987, *MNRAS*, 227, 1
- Ariel Keselman, J. & Nusser, A. 2007, *MNRAS*, 382, 1853
- Lacey, C., & Cole, S. 1993, *MNRAS*, 262, 627
- Landy, S. D., & Szalay, A. S. 1993, *ApJ*, 412, 64
- Mo, H. J., & White, S. D. M. 1996, *MNRAS*, 282, 347
- Peacock, J. A., & Smith, R. E. 2000, *MNRAS*, 318, 1144
- Sandvik, H. B., Möller, O., Lee, J., & White, S. D. M. 2007, *MNRAS*, 377, 234
- Scoccimarro, R., Sheth, R. K., Hui, L., & Jain, B. 2001, *ApJ*, 546, 20
- Seljak, U. 2000, *MNRAS*, 318, 203
- Skibba, R., Sheth, R. K., Connolly, A. J., & Scranton, R. 2006, *MNRAS*, 369, 68
- Springel, V. 2005, *MNRAS*, 364, 1105
- Springel, V., Yoshida, N., & White, S. D. M. 2001, *New Astronomy*, 6, 79
- Tinker, J. L. 2007, *MNRAS*, 374, 477
- Tinker, J. L., Conroy, C., Norberg, P., Patiri, S. G., Weinberg, D. H., & Warren, M. S. 2007, *ArXiv e-prints*, 707
- Tinker, J. L., Weinberg, D. H., & Zheng, Z. 2006, *MNRAS*, 368, 85
- van den Bosch, F. C., Mo, H. J., & Yang, X. 2003, *MNRAS*, 345, 923
- Wang, H. Y., Mo, H. J., & Jing, Y. P. 2007, *MNRAS*, 375, 633
- Wechsler, R. H., Bullock, J. S., Primack, J. R., Kravtsov, A. V., & Dekel, A. 2002, *ApJ*, 568, 52
- Wechsler, R. H., Zentner, A. R., Bullock, J. S., Kravtsov, A. V., & Allgood, B. 2006, *ApJ*, 652, 71
- Weinmann, S. M., van den Bosch, F. C., Yang, X., Mo, H. J., Croton, D. J., & Moore, B. 2006, *MNRAS*, 372, 1161
- Wetzel, A. R., Cohn, J. D., White, M., Holz, D. E., & Warren, M. S. 2007, *ApJ*, 656, 139
- White, S. D. M. 1996, in *Cosmology and Large Scale Structure*, ed. R. Schaeffer, J. Silk, M. Spiro, & J. Zinn-Justin, 349–+
- Yang, X., Mo, H. J., & van den Bosch, F. C. 2003, *MNRAS*, 339, 1057
- 2006, *ApJ*, 638, L55
- York, D. G., & et al. 2000, *AJ*, 120, 1579
- Yoo, J., & et al. 2006, *ApJ*, 652, 26
- Zehavi, I., Zheng, Z., Weinberg, D. H., Frieman, J. A., Berlind, A. A., Blanton, M. R., Scoccimarro, R., Sheth, R. K., Strauss, M. A., Kayo, I., Suto, Y., Fukugita, M., Nakamura, O., Bahcall, N. A., Brinkmann, J., Gunn, J. E., Hennessy, G. S., Ivezić, Ž., Knapp, G. R., Loveday, J., Meiksin, A., Schlegel, D. J., Schneider, D. P., Szapudi, I., Tegmark, M., Vogeley, M. S., & York, D. G. 2005, *ApJ*, 630, 1
- Zentner, A. R. 2006, *ArXiv Astrophysics e-prints*
- Zhao, D. H., Mo, H. J., Jing, Y. P., & Börner, G. 2003, *MNRAS*, 339, 12
- Zheng, Z. 2004, *ApJ*, 610, 61
- Zheng, Z., Berlind, A. A., Weinberg, D. H., Benson, A. J., Baugh, C. M., Cole, S., Davé, R., Frenk, C. S., Katz, N., & Lacey, C. G. 2005, *ApJ*, 633, 791
- Zheng, Z., & Weinberg, D. H. 2007, *ApJ*, 659, 1
- Zheng, Z., Coil, A. L., & Zehavi, I. 2007, *ApJ*, 667, 760
- Zhu, G., Zheng, Z., Lin, W. P., Jing, Y. P., Kang, X., & Gao, L. 2006, *ApJ*, 639, L5